Sudan University of Science and Technology
Collage of Graduate Studies

# Effect of pH on Structural and Optical Properties of Magnesium Chromates Nanocrystals Synthesized by Combustion Method

## تأثير الرقم الهيدروجيني على التركيب و الخصائص البصرية لبلورات كرومات المغنيسيوم النانوية المحضرة بطريقة الإحتراق

**A Dissertation Submitted in Partial Fulfillment for the Requirement of a Master Degree (M.Sc) in Physics**

## Prepared by

**HAFAWA KABBASHI NASIR HAJANI**

## Supervised by

**Dr. NADIR S.E. OSMAN**

**October 2020**

# الآية

**بسم الله الرحمن الرحيم**

**(قَالُوا سُبْحَانَكَ لَا عِلْمَ لَنَا إِلَّا مَا عَلَّمْتَنَاۖ إِنَّكَ أَنتَ الْعَلِيمُ الْحَكِيمُ)**

**صدق الله العظيم**

**البقرة الآية (32 )**

# Dedication

*I would dedicate to*

***My family***

*Support me and show me the best path to follow*

*And*

***Especially to my father***

The words are racing and crowded to organize the thanks giving, who amazing and I am lucky to have you .He constantly encourage me and did not wait tender.

*And*

***To my dear loved mother***

There are not enough words I can say to describe her, she gave me life which is worthy of God's mercy.

# Acknowledgments

First and foremost, praises and thanks to God, the Almighty, for His showers of blessings throughout my research work to complete this research successfully.

I would like to express my deepest and sincere gratitude to my research supervisor, **Dr. NADIR S.E. OSMAN** for providing invaluable guidance throughout this research. His dynamism, vision, sincerity and motivation have deeply inspired me. He has taught me the methodology to carry out the research and to present the research works as possible. It was a great privilege to work and study under his guidance.

I also would like to acknowledge Africa City of Technology for providing equipment that was used to synthesize the materials for this work. Furthermore, many thanks are due to staff members of the Department of Physics at Sudan University of Science and Technology for being as a family.

Finding each other has been a journey I cannot express enough thanks to my friends **Fatima Hayder**, **Nuha Abdullah** and **Wlaa. Wlaa**, I'm so lucky to have you in it my life. You may not share my DNA, but you share my heart. Happiness is to have great friends like you.

Last but not least, I would like to thanks all the professors of the Sudan University of Science and Technology.

Finally, I must express very profound gratitude to my parents, my sisters, my brothers and my friends for providing me with unfailing support and continuous encouragement throughout my study and through the process of researching and writing this thesis. This accomplishment would not have been possible without them.

# Abstract

In this work magnesium chromate ($MgCr_2O_4$) samples were produced by combustion method. Sample 1 was prepared without adding ammonia hydroxide (pH = 0.96) during synthesis steps whilst sample 2 was prepared with ammonia hydroxide (pH = 8.62). Sample 1 was obtained in 2:10 h whilst sample 2 was produced in 45 min. Effect of pH upon structural properties were investigated by X-rays diffraction (XRD) technique. The results confirm the formation of the cubic spinel structure with average crystallite sizes of 13.0 nm and 8.0 nm for sample 1 and sample 2, respectively. The lattice parameters were calculated using Bragg's law and found to be 8.30 Å and 8.33 Å for sample 1 and sample 2, respectively. The X-rays densities values were $2.227\times 10^6$ g/cm$^3$ and $2.206\times 10^6$ g/cm$^3$ for the sample 1 and sample 2, respectively. The obtained microstrain values were 0.007148 and 0.015206 for sample 1 and sample 2, respectively. The optical properties were studied using Ultra violate -Visible (Uv-Vis) absorption technique. The results show that $MgCr_2O_4$ samples have a direct band gap of 3.007 eV and 3.057 eV for the sample 1 and sample 2, respectively. It observed that the band gap of sample 2 was slightly greater compared to sample 1. This associated with crystallite sizes of the samples. It can be concluded that control of pH can significantly reduce the duration of combustion synthesis method.

# المستخلص

في هذا البحث تم انتاج عينات كرومات الماغنيسيوم بطريقة الإحتراق، حيث تم تحضير العينة الأولى بدون إضافة أمونيا هيدروكسيد ( pH =0.96) خلال التحضير، العينة الثانية حضرت بإضافة أمونيا هيدروكسيد (pH = 8.62). تم الحصول على العينة الأولى في 2:10 ساعة بينما العينة الثانية تم الحصول عليها في 45 دقيقه. تمت دراسة تأثير الرقم الهيدروجيني علي الخواص التركيبية بإستخدام تقنية حيود الأشعة السينية. أكدت نتائج إنحراف الأشعة السينية تكون المادة بحجم بلوري يعادل 13.05 و7.84 نانومتر للعينة الأولى والثانية علي التوالي. تم حساب معامل الشبيكة بقانون براغ ووجد انه يساوي 8.30 و8.33 انجستروم للعينة الأولى والثانية علي التوالي. قيم كثافة الأشعة السينية $2.227\times 10^{6}$ جم/سم$^3$ **و** $2.206\times 10^{6}$ جم/سم$^3$ للعينة الأولى والثانية علي التوالي. قيم الإجهاد المتحصل عليها 0.007148 و0.015206 للعينة الأولى والثانية علي التوالي.
تمت دراسة الخصائص البصرية بإستخدام تقنية إمتصاص الأشعة فوق البنفسجية-المرئية حيث أظهرت النتائج أن عينات مركب كرومات الماغنيسيوم لها فجوة نطاق مباشرة تساوي 3.007 الكترون فولت و3.057 الكترون فولت للعينة الأولى والثانية علي التوالي. لوحظ أن فجوة النطاق للعينة الثانية أكبر قليلا مقارنة بالعينة الأولى. وهذا مرتبط بأحجام البلورات للعينات. يمكن الإستنتاج أن التحكم في الرقم الهيدروجيني يمكن أن يقلل بشكل كبير من مدة التحضير بطريقة الإحتراق.

## Keywords and acronyms

## Keywords

Synthesized, Combustion, magnesium chromate, optical properties, PH meter.

## Acronyms

Magnesium chromate ($MgCr_2O_4$).
X-rays diffraction (XRD).
Ultra violate –Visible (Uv-Vis) spectroscopy.
Fourier transforms infrared spectroscopy (FTIR).

# Table of Contents



## CHAPTER ONE

## INTRODUCTION

## CHAPTER TWO

## THEORETICAL BACKGROUND



## CHAPTER THREE

## EXPERIMENTAL DETAILS



## CHAPTER FOUR

## RESULTS AND DISCUSSION

# List of figures

# CHAPTER ONE

# INTRODUCTION

## 1.1 General overview

The term nano originated from Greek word nanos which means ‘dwarf’. It uses to describe very small objects, particularly one billionth of a meter (Boholm, M. 2012). Materials at nano scale have unique optical, mechanical, electrical and magnetic properties compared to their bulk sizes (Jaison, J. et al. 2018). This stimulated researches to understand the behavior of naomaterials which can lead to promising applications. Consequently, nanoscience associated with the study of matter at the nanoscale in order to understand their sizes and structure-dependent properties (Jaison, J. et al. 2018). Further, nanotechnology concerns with obtaining of functional nanomaterials as well as devices that fabricated based on nanoscience (Roco, M. C. 1999). This produces interesting wide range of applications in different field such as nano electronics, chemical engineering, agriculture, industry, biotechnology, medicine and environmental technology (Shapira, P. and Jan, Y. 2011).

Nanomaterials with at least one dimension less than 100 nm can be described as nanocrystals which composed of atom in either a single or poly-crystalline arrangement (Wurschum, R. and Schaefer, H. E. 1996, Burt, J. L. 2005). Physical and chemical properties of these types of materials show strong size dependent that associated with quantum size effect (Fahlman, B. D. 2007). Therefore, many researchers have been attracted to investigate their behavior due to possible potential applications

such as in optical and bio medicals fields (Wurschum, R. and Schaefer, H. E. 1996).

Metal oxides nanocrystals are considered one of the most important classes of materials and have different electrical properties from metals, semiconductors and insulators (Chen, H. M. and Liu, R. S. 2011). This make them used in many different applications such as sensors and superconductors. However, depending on the structure, metal oxides mainly can be classified into Peroviskite or Spinel oxides (Sumaira, N. 2016).

### 1.2 Spinel oxides

The word spinel has been derived from Italian word spinella, means spiky crystal, Spinel structure was discovered by Bragg in 1915 (Suzuki, N. et al. 2008). Materials with this type of structure have shown remarkable mechanical, electrical, optical and magnetic properties (Stanojević, Z. M. et al. 2007), thus they are appropriate for many technological applications, such as superconductors (Ueda, N. et al. 1992), magnetic cores (D. Johnston, et al. 1973) and high-frequency devices (Gorter, E. W. 1954). Properties of spinel oxides are highly influenced by type of atoms and their position in the crystal structure (Suzuki, N. et al. 2008).

### 1.3 Spinel structure

Spinel structure have the formula $AB_2O_4$ where $A$ is the divalent ions (such as $Zn^{+2}$, $Mg^{+2}$ and $Ni^{+2}$) occupy the tetrahedral sites and $B$ is the trivalent ions (such as $Fe^{+3}$, $Cr^{+3}$ and $Al^{+3}$) occupy the octahedral sites in a close packed arrangement of oxide ions (Manjon, F. J. et al. 2014). The cations occupy only one-eighth of the tetrahedral sites and one-half of the octahedral sites as shown in figure 1.1. Unit cell of spinels structure belongs to cubic

structure with space group *F3dm* and presented in the cubic form $AOB_2O_3$ by eight molecules and comprising of 32 $O^{-2}$ anions (Grimes, N. W. 1983). These oxygen anion from the close face-centered cube (FCC) packing which is contained in 64 tetrahedral (*A*) and 32 octahedral (*B*) empty spaces partially occupied by $B^{3+}$ and $A^{2+}$ cations conferring to the distribution of cations, three types of spinel structures namely normal, inverse and mixed spinel (Grunes, L. 1983).

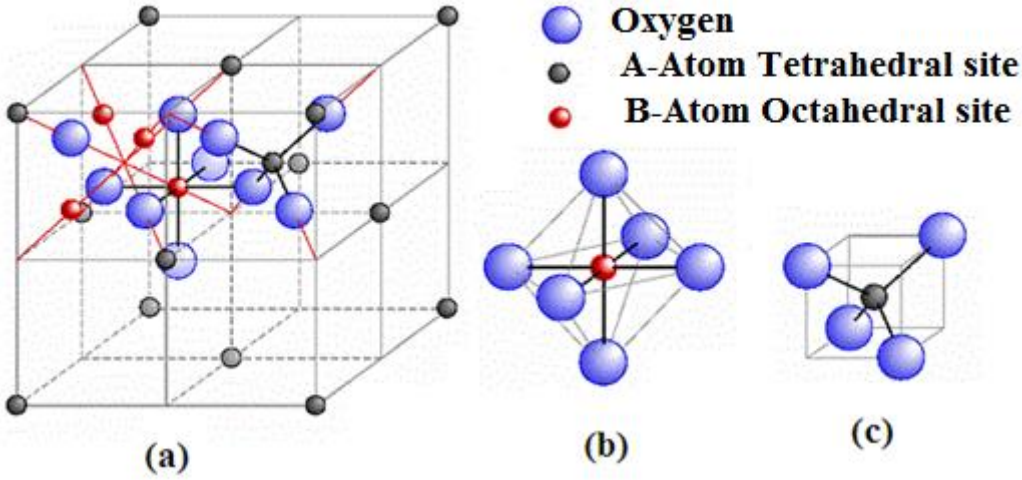


Figure 1.1. Graphic representation of (a) spinel structure unit cell, (b) octahedral and (c) tetrahedral sites.

### 1.3.1 Normal spinels

In normal spinel structures, all the divalent ions occupy the *A* sites. For example the structural formula of normal chromates is $A^{2+}$ $[Cr_2^{+3}]$ $O_4^{2-}$. Particularly, this type of distribution can be observed in magnesium chromates as $Mg^{2+}$ $[Cr^{2+}$ $Cr^{3+}]$ $O_4^{2-}$ (Burdett, J. K. et al. 1983).

### 1.3.2 Inverse spinels

This type of spinel structure represented as $B^{3+}$ $[A^{2+}\ B^{3+}]\ O_4^{-2}$, all the $A^{2+}$ and half of $B^{3+}$ cations are in octahedral sites and the other half of $B^{3+}$cations are in tetrahedral sites (Bates, J. L. and Gamier, J. E. 1981). Particularly, this type of distribution can be observed in magnesium chromates as $Cr^{3+}$ $[Mg^{2+}Cr^{3+}]\ O_4^{2-}$ (Burdett, J. K. et al. 1983).

### 1.3.3 Mixed spinels

The general formula of this type of spinel structure can be represented as $(A_{1-x}\ B_x)\ (A_x\ B_{2-x})\ O_4^{2-}$, *A* and *B* both sites distributed randomly over the available tetrahedral and octahedral voids, For example the structural formula of mixed chromates is $A_{1-x}^{2+}\ Cr_x^{3+}\ [A_x^{2+}\ Cr_{2-x}^{3+}]\ O_4^{2-}$, where the degree of inversion is given by *x* (Burdett, J. K. et al. 1983).

## 1.4 Chromite

This metal oxide belongs to the spinel group (Routschka, G. and Wuthow, H. 2008). Chromite has been the key raw material in the production of chromium chemicals since the early 19$^{th}$ centuries. It used for the advanced production of biocides, catalysts, pigments, corrosion inhibitors, chemicals used in oil fields, plating and highly pure chromium metal, also used in the production of printing chemicals (White, A. D. 2006).

Transitional metal chromates have significant implications on the foundation of a wide range of materials due to their performance at high-pressure conditions. Among chromate materials pirochromite ($MgCr_2O_4$) can be used in different technological applications, such as strengthening agents, sensor

elements, interconnecting materials for solid oxide fuel cells and combustion catalysts (Sanjeeviraja, G. and Kalai, S. 2013).

### 1.5 Synthesis approaches of nanomaterials

Synthesis method plays significant role in determining the properties of nanomaterials. Generally, two synthesis approaches have been reported in literature known as top-down and bottom-up.

#### 1.5.1 Top-Down approach

The most common technique of top-down for producing nanomaterials is mechanochemical milling of micron or bulk scale materials. In this case, larger particles are broken down to smaller ones (Manh, D. H. et al. 2009).

#### 1.5.2 Bottom-Up approach

The bottom-up approach generally creates larger structures starting from atom or molecular (Rotello, V. M. 2004). The main examples of bottom-up approach are wet chemical synthesis methods. This includes hydrothermal, combustion, gas-phase, microwave and sol-gel processing.

Several important factors that crucial in synthesis of nanomaterilas include stachometric, temperature and pH of the solution (Baker, S. et al. 2013). Researchers have discovered that pH of the solution medium can affect the size and morphology of the nanomaterilas (Armendariz, V. et al. 2004).

## 1.6 Literature review

Several researchers have procedure their efforts to improve the properties of spinel chromates.

Ehsan Jafarnejad et al (2016) synthesized pirochromite samples by stearic acid sol-gel method. The characterization of $MgCr_2O_4$ nanocrystalline were carried out by X-ray diffraction spectroscopy (XRD), electron dispersive X-ray spectroscopy (EDX), scanning electron microscope (SEM), Fourier transform infrared spectroscopy (FT-IR) and diffuse reflectance spectroscopy (DRS). Experimental results show that the average particle sizes of the $MgCr_2O_4$ were in the range of 39 nm to 71 nm. The obtained band-gap was approximately 1.8 eV.

Fathalla Hamed (2016) synthesized nanostructured pirochromite using fresh and boiled egg shell membranes (ESM). The obtained nanocrystalline $MgCr_2O_4$ powders were characterized by XRD, FTIR, SEM, EDS (Energy dispersive X-ray spectrometry**)** and UV-Vis-NIR spectrometry. $MgCr_2O_4$ powders were subjected to heat treatment at 1000 ºC for 4 h to produce single phase structure. The average of crystallite sizes were 63.2 nm, 46.9 nm and 64.5 nm for Un-templated, boiled ESM templated and Fresh ESM template, respectively. The values of lattice constants of the 1000 ºC annealed were 8.347 Å, 8.323 Å and 8.324 Å, for Un-templated, boiled ESM templated and Fresh ESM template, respectively. The optical properties measurements show that the synthesized $MgCr_2O_4$ samples possessed a direct band gap.

## 1.7 Problem statement

Synthesis of nanomaterials using wet chemical methods is considered to be tedious and take relatively long time. However, control of pH is expected to decrease duration of combustion synthesis method.

## 1.8 Aim of this research

This work aims to decrease duration of synthesis procedures of combustion method. The aim extends to investigate the effect of pH on structural and optical properties of magnesium chromate samples.

## 1.9 Objectives

### Main objective

- To synthesize magnesium chromate samples using combustion method with control of pH.

### General objective

- To identify the formation of spinel structural of the synthesized samples using X-rays diffraction spectroscopy.

- To identify the functional group of the synthesized magnesium chromate samples using Fourier transform infrared spectroscopy.

- To investigate the band gap of the synthesized magnesium chromate samples using ultraviolet -visible spectroscopy.

### 1.10 Dissertation outlines

This dissertation consists of four chapters. Introduction of nano, summary of metal oxides, a brief discussion on the general background of spinel structure, in addition to the literature review, problem statement and objectives, in chapter one. The theoretical background of optical properties of materials was explained in Chapter two. Chapter three presents the detailed procedures that were involved in combustion synthesis method.

Chapter four devoted to the results and discussion, conclusions, recommendations and future work.

# CHAPTER TWO

# THYORATICAL BACKGROUND

This chapter discusses theoretical background of structural and optical properties of the synthesized samples.

## 2.1 X-rays diffraction spectroscopy (XRD)

X-rays diffraction is a technique that can be used for phase identification. It is suitable for crystalline substances. The interaction of the incident X-rays with a crystalline sample produces constructive interference when Bragg's law is satisfied. In this technique the diffracted X-rays are then detected, processed and counted. Scanning a powdered sample through a range of $2\theta$ angles, all possible diffraction directions of the lattice can be attained. XRD measurements can used to obtain structural properties such as lattice parameters, crystallite sizes, density and microstrain (Brindley, G. W. Brown, G. 1980). Figure 2.1 shows reflection of X- rays from crystal planes.

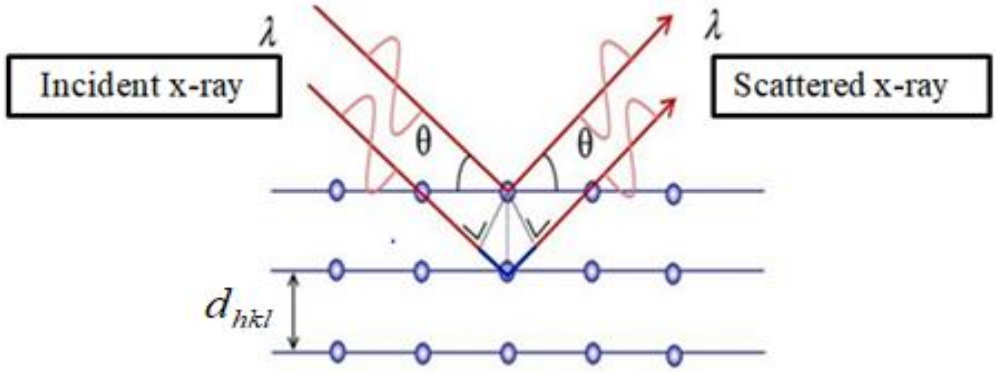


**Figure 2.1.** Schematic illustration of X- rays diffraction by a crystal.

Lattice parameters refer to the physical dimension of the unit cell in a crystal lattice. Lattices in three dimensions generally have three lattice constants, referred to as *a*, *b*, and *c* (Ahmed, M. A. 2011). However, in cubic crystal structures the lattice parameter (*a*) can be calculated from the XRD spectra by using the equation

$$a = \frac{\lambda}{2\sin\theta}\sqrt{(h^2 + k^2 + l^2)}, \qquad 2.1$$

where *h*, *k* and *l* are Miller indices.

The crystallite sizes (*D*) can be calculated using Scherrer's formula given

$$D = \frac{k\lambda}{\beta\cos\theta}, \qquad 2.2$$

where *K* is the Scherrer's constant takes the value of 0.94 for spherical crystals with cubic symmetry, $\lambda$ is the X-rays wavelength, $\beta$ is the full width half maximum (FWHM) of the highest intensity peak and $\theta$ is the Bragg's angle (Kakani, S. L. and Amit, K. 2004).

The X-rays density ($\rho_{XRD}$) of a sample can be determined using the relation produced by Smith and Wijn (Smith, J. and Wijn, H. 1959)

$$\rho_{XRD} = \frac{8M}{N_a a^3}, \qquad 2.3$$

where *M* is the molecular weight of the composition and $N_a$ is the Avogadro's number.

The micro strain ($\varepsilon$) can be calculated from the equation (Mariappan, R. 2012)

$$\varepsilon = \frac{\beta}{4\tan\theta}, \qquad 2.4$$

## 2.2 Optical properties

Optical properties include optical absorption, optical band gap and quantum size effect of nanomaterials are significantly affected by many factors such as doping, shape and particles sizes **(**Wolcott, A. et al. 2006)**.**

### 2.2.1 Optical absorption

The absorption of the light waves depends on the wavelength of the light, the thickness of the absorber or the transmitted media and the nature of the media. The absorption associated with comparison between intensities of incident light *I* and transmitting light $I_0$ through a sample. Optical absorption *A* of a material can be obtained using Beer-Lamberts law (Gratzel, M. 1988).

$$A = \log\frac{I_0}{I} = e^{-\alpha x}, \qquad 2.5$$

where $\alpha$ is absorption coefficient, *x* is a thickness of sample.

### 2.2.2 Quantum size effect

Most of remarkable properties of nanomaterial are attributed to quantum confinement effect which is essentially due to changes in the atomic structure as a result of direct influence of nanosize on the energy band structure (Xinyuan, Z. et al. 2004). The quantum confinement effect can be qualitatively explained using the effective mass approximation for a spherical particle with radius *R*, the effective band gap $E_g$ effective (R) is given by equation

$$E_g \text{effective}(R) = E_g(\infty) + \frac{h}{2R^2} + \frac{1}{M_e} + \frac{1}{Mh} - \frac{1.8e^2}{\varepsilon R}, \qquad 2.6$$

where $E_g(\infty)$ is the bulk band gap, $m_e$ and $m_h$ are the effective masses of the electron and hole, and $\varepsilon$ is the bulk optical dielectric constant or relative permittivity. The first term in this equation is the band gap of the bulk semiconductor (Bawendi, M. et al. 1990). The second term shows that the effective band gap is inversely proportional to $R^2$. This implies that effective band gap increases as particles size decreases. However, since the second term becomes dominant at small $R$, the effective band gap is expected to increase with decreasing $R$, particularly when $R$ is small.

This illustrates in figure 2.2 dependence of the band gap on the size of quantum dots. The third term shows that the band gap energy decreases with decreasing $R$ due to increase of Coulombic interaction (Hodak, J. et al. 1998).

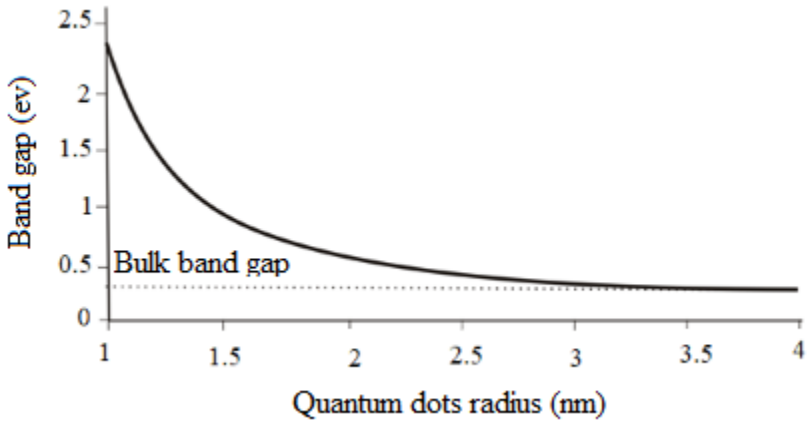


**Figure 2.2.** Sillustration of dependence on band gap to the size of quantum dots.

## .23.Optical band gap

The optical band gap energy depends on the absorption coefficient as described by the relations

$$\alpha h\nu = B(h\nu - E_g)^n, \qquad 2.7$$

*B* is constant independent of wavelength gives a satisfactory description of the absorption behavior in this wavelength domain, *hν* is incident photon energy, *h* is the Planck constant. For direct transition n=2 for allowed transition, $E_g$ is direct energy gap and n=1/2 for indirect transition, $E_g$ is indirect energy gap (Cheng, P. and Lian, G. 2008).

# CHAPTER THREE
# EXPERIMENTAL DETAILS

This chapter describes synthesis method and the experimental procedures that were used for structural and optical characterizations of the samples. Two magnesium chromate samples with different pH were synthesized using combustion method. Sample 1 was prepared without ammonium hydroxide (pH = 0.96) whilst sample 2 was prepared with ammonium hydroxide (pH = 8.62).

## 3.1 Synthesis of magnesium chromate samples

Combustion synthesis method is commonly used for producing monodispars metal oxide nanocrystal powders (Adair, J. H. et al 1998). It is considered as simple, fast and producing high quality materials (Houshiar, M. et al 2013). This method requires fuel such as urea for the reaction to occur. In this work, sample 1 was prepared by dissolving 7.0 g of Mg $(NO_3)_3.6H_2O$, 10.60 g of Cr $(NO_3)_2.9H_2O$ and 8.20 g of $CH_4N_2O$ in 50 ml of deionized water to form a clear aqueous solution. The paste formed was evaporated on a hot plate at 70 ºC. After 1:50 h temperature was raised up to 100 ºC until a thick gel was obtained. The temperature was raised up to 350 ºC for the auto combustion reaction. The final powder obtained after 2:10 h was in a Pale green color. Figure 3.1 shows the experimental set up of the combustion method for sample1 at 350 ºC.

**Figure 3.1.** Experimental set up of the combustion method for sample 1 at 350 ºC, Institute of Laser, Sudan University of Science and Technology, Sudan.

Sample 2 was prepared by dissolving 7.0 g of Mg $(NO_3)_3.6H_2O$, 10.60 g of Cr $(NO_3)_2.9H_2O$ and 8.20 g of $CH_4N_2O$ in 50 mL of deionized water to form a clear aqueous solution. The paste formed was evaporated on a hot plate at 70 ºC. After 10 minute the $NH_4OH$ was added slowly to the solution. Initially, pH was 1.8 as measured by pH meter and after adding of the ammonium hydroxide to the mixture, it color changed from green to gray. After 6 minute the temperature was raised up to 350 ºC and pH raise to 8.62 until a thick gel was obtained. Finally, dusky gray powders were obtained after 45 minute. Figure 3.2 shows the experimental set up of the combustion method for sample 2 at 350 ºC.

**Figure 3.2.** Experimental set up of the combustion method for sample 2 at 350 ºC, Research Lab, Sudan University of Science and Technology, Sudan.

## 3.2 Characterization techniques

The synthesized magnesium chromate samples were characterized using X-ray diffraction (XRD), Fourier transform Infrared spectroscopy (FT-IR) and Ultraviolet -Visible spectroscopy (UV-Vis).

### 3.2.1 X-rays diffraction spectroscopy

The structural characterization of the synthesized magnesium chromate samples were performed using X-rays diffractometer D8-Advance from Bruker operated in a continuous $\theta$-$\theta$ scan in locked coupled mode with $CuK_{\alpha}$ radiation. The sample is mounted in the center of the sample holder on a glass slide and leveled up to the correct height. The measurements run within a range in $2\theta$ defined by the user with a typical step size of 0.034° in $2\theta$. A sensitive detector, Lyn-Eye was used to record diffraction data at a typical speed of 0.5 sec/step which is equivalent to an effective time of 92 sec/step for a scintillation counter. Figure 3.3 shows the X-rays diffractometer that was used in this work.

**Figure 3.3.** The X-rays diffractometer D8-Advance from Bruker AXS (Germany) operated South Africa.

### 3.2.2 Fourier transforms infrared (FT-IR) spectroscopy

Fourier transform infrared (FT-IR) spectroscopy analysis is used to identify chemical bonds in samples (Cui, H. et al. 2017). In terms of wave numbers, the vibrational infrared extends from about 4000 to 400 $cm^{-1}$.

The basic components of FT-IR includes a source (black-body), collimator, beam splitter (mirror), fixed mirror, moving mirror, sample compartment, laser for aligning the mirrors as well as for internal calibration and detector. Figure 3.4 shows a simple schematic diagram of FT-IR instrument.

The basic principle of FT-IR is based on the molecular bonds vibration at various frequencies. This depends on the elementals compositions and type of bonds however, only specific frequencies can cause bonds vibration. These selected frequencies are corresponding to the ground state and excited states of the sample. The bonds vibration can be achieved by absorption of process infrared radiation (Salahudeen, A. G. 2014).

This because the energy corresponds to the transitions between molecular vibrational states is generally 1-10 kilocalories/mole which lien in the infrared region on the electromagnetic spectrum (Salahudeen, G. 2014). In this work, the FT-IR measurements of the synthesized samples were performed using the computer which then presents the user with the desired spectral information for analysis as shown in Figure 3.5.

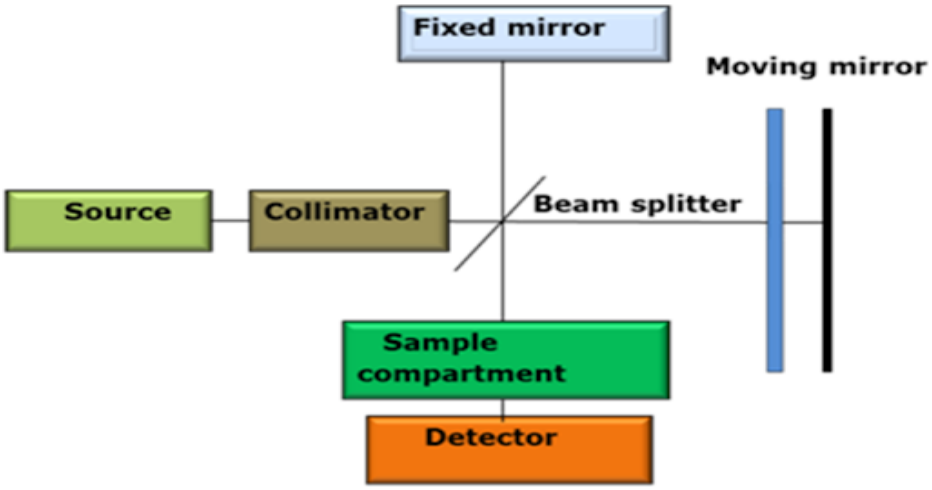


**Figure 3. 4.** Schematic diagram illustrates the FT-IR instrument.


**Figure 3.5.** Fourier transforms Infrared (FT-IR) IR Tracer 100 spectrometer, Forensice, Sudan.

### 3.2.4 Ultraviolet-Visible spectroscopy

Figure 3.6 describes principle of UV-Visible spectrometer where, a beam of light from UV-Visible light source is separated into its component wavelengths by a prism or diffraction grating. A half mirrored is used to split each monochromatic beam into two equal intensity beams namely sample and reference beams. The sample beam passes through small transparent container (cuvette) containing a solution made of the compound under investigation in a transparent solvent. The reference beam passes through an identical cuvette containing only the solvent $CH_3CH_2OH$. The intensities of reference beam $I_0$ and sample beam $I$ are then measured by photo detectors and compared (Salahudeen, A. G. et al. 2014).

The spectrometer scans the ultraviolet region from 200 to 400 nm, visible region from 400 to 800 nm and infrared region beyond 800 nm. In the case of on light is absorbed by the sample. Absorption can be describes as transmittance ($T = I/I_o$) or absorbance ($A = \log I_o/I$). In this case of no light is absorbance by the sample, then T = 1.0 and A= 0. Most spectrometers display absorbance on the vertical axis and the commonly observed range is from 0 (100% transmittance) to 2 (1% transmittance) (Salahudeen, A. G. et al. 2014). The wavelength of maximum absorbance is a characteristic value of UV-Visible spectrometer designated as λmax (Salahudeen, A. G. et al. 2014).The optical properties of the synthesized samples were investigated using Ultra-Violet- Visible (UV-Vis) spectrometer as show figure 3.7.

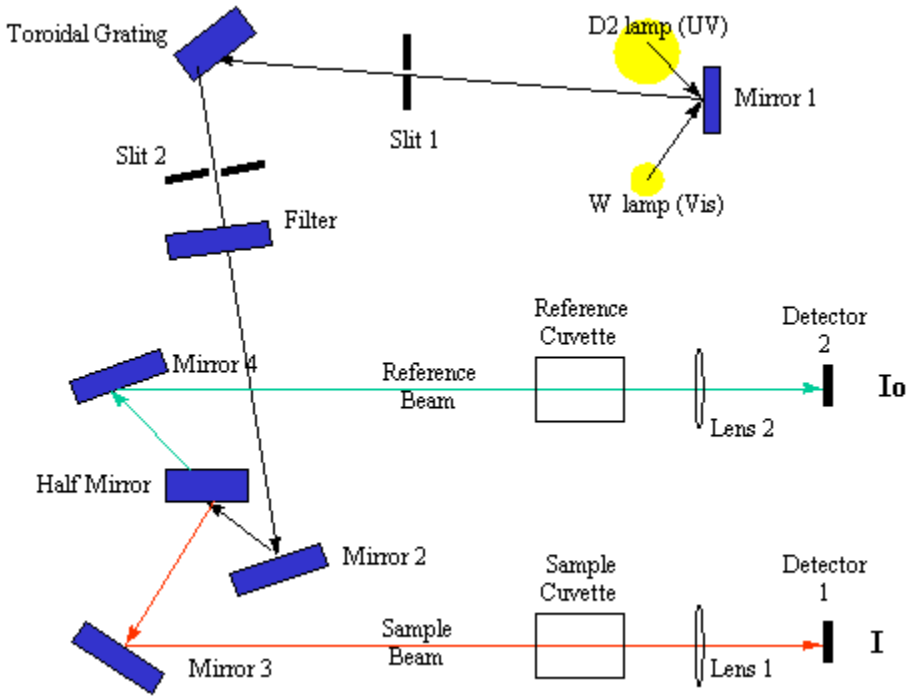


**Figure 3.6.** Schematic diagram illustrates the principle of UV-Visible spectroscopy (Smith, 1978).


**Figure 3.7.** Ultra violet -Visible (Uv-Vis) spectrometer 7205, Research lab, Sudan University of Science and Technology, Sudan.

# CHAPTER FOUR

# RESULTS AND DISCUSSION

This chapter presents and discusses the structural and optical properties of the synthesized magnesium chromate ($MgCr_2O_4$) samples. Two samples designated as sample 1 and sample 2, were synthesized using combustion method. Sample 1 was prepared without adding ammonia hydroxide during synthesis steps whilst, sample 2 was prepared with ammonia hydroxide.

## 4.1 X-rays diffraction results of the synthesized magnesium chromate ($MgCr_2O_4$) samples

The structure and phase formation of the synthesized magnesium chromate samples were studied by X-rays diffraction (XRD) technique. Figure 4.1 shows the XRD patterns of sample 1 and sample 2. Data were collected in the range of $10° < 2\theta < 130°$ with CuK$\alpha$ of 0.154 nm at room temperature. As shown in the figure, the prominent diffraction peaks are well indexed. The main peak that corresponding to the crystal plane with Miller indices (311) was centered at $2\theta = 35.72°$ and $2\theta = 35.60°$ for sample 1 and sample 2, respectively, which confirms the presence of spinel $MgCr_2O_4$ with a cubic face structure (Ghead, K. and Saja, M. 2016). From figure 4.1 the sharpness of XRD patterns reflect that sample 1 show good crystallinty compared to sample 2. The broadening of XRD peaks indicates that the crystallite sizes of sample 2 are greater compared to sample 1.

The lattice parameters ($a$) were calculated from the XRD data using equation 2.1. The calculated lattice parameters were 8.30 Å and 8.33 Å for sample 1 and sample 2, respectively. The lattice parameters of sample 2 slightly larger

compared to sample 1. This associated with duration of synthesis procedures which expect to have influence on the strain of the unit cell of the sample.

The average crystallite sizes ($D$) were determined using Scherer's formula as in equation 2.2. The calculated average values were 13.0 nm and 8.0 nm for sample 1 and sample 2, respectively. The value of crystallite sizes of sample 1 are larger compared to sample 2. This associated with the duration of synthesis process (Tholkappiyan, R. and Fathalla, H. 2016), since sample 1 took more time before combustion reaction occured. Therefore, it expected to have grater crystallite sizes.

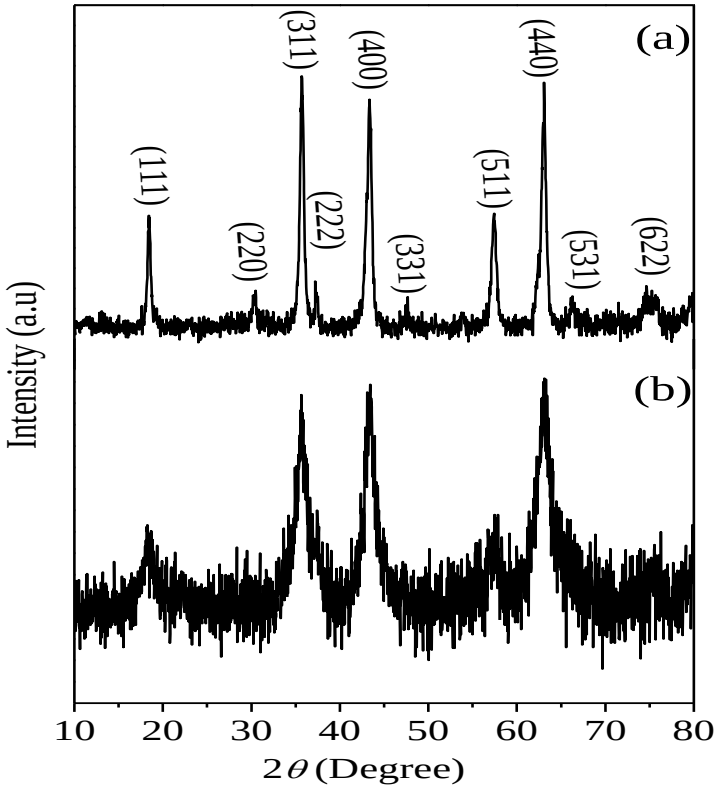


**Figure 4.1.** XRD patterns of (a) sample 1 and (b) sample 2.

The X-rays densities ($\rho_{XRD}$) of the synthesized $MgCr_2O_4$ samples were determined using equation 2.3. The calculated values were $2.227\times 10^6$ g/cm$^3$ and $2.206\times 10^6$ g/cm$^3$ for the sample 1 and sample 2, respectively.

The microstrain ($\varepsilon$) values were calculated using equation 2.4. The obtained values were 0.007148 and 0.015206 for sample 1 and sample 2, respectively. Since sample 2 possesses larger value of lattice parameter therefore, it expected to have greater value of microstrain compared to sample 1.

## 4.2 FT-IR results of the synthesized magnesium chromate ($MgCr_2O_4$) samples

The functional groups of the synthesized magnesium chromate samples were identified using the Fourier transform infrared (FT-IR) spectroscopy. A particular vibration frequency range can be assigned to a bond type due to the fact that specific frequencies are absorbed by the molecules of a material which are characteristic of their structure. The frequency of the absorbed radiation is assigned to the bond or group that vibrates.

Figure 4.2 shows the FTIR results of sample 1. The data were collected in the range of 480-4000 $cm^{-1}$. The peak at 2358.94 $cm^{-1}$ is associated with O-H vibration from the Alcohols group, the appearance of the peak at 1653.00 $cm^{-1}$ is attributed to N-H bending vibration from the Amine group, the peak at 1558.48$cm^{-1}$ is associated C=C with stretching vibration from the Alkenes group, the peak at 1506.41 $cm^{-1}$ is associated with N-O asymmetric stretching vibration from the Nitro compounds, (Loría-Bastarrache, W., et al. 2011), The absorption peak of Cr-O bonds observed at 630.72 $cm^{-1}$. Similar results have been reported by Salahudeen et al (Salahudeen, A. G. et al. 2014).

Figure 4.3 shows the FTIR results of sample 2. The peak at 2345.44 $cm^{-1}$ is associated with O-H vibration from the Alcohols group, the appearance of the peak at 1695.43 $cm^{-1}$ is attributed to C=O stretching vibration from the

Ketones group, the peak at 1653 $cm^{-1}$ is attributed to N-H bending vibration from the Amine group, the peak at 1558.48$cm^{-1}$ is associated with C=C stretching vibration from the Alkenes group, the peak at 1533.41 $cm^{-1}$is associated with N-O bend vibration from the Nitro compounds, (Loría-Bastarrache, W., et al. 2011), while the absorption peaks of Cr-O bonds observed at 628.79 $cm^{-1}$ (Salahudeen, A. G. et al. 2014).

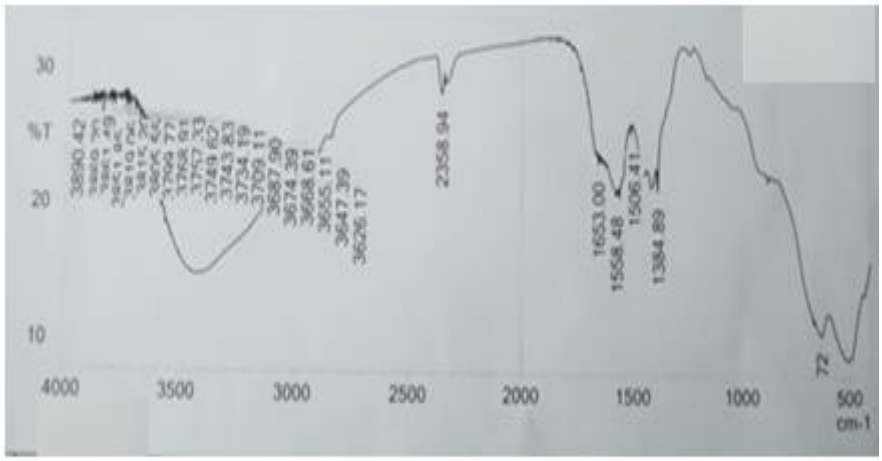


**Figure 4.2.** FT-IR spectrum of sample 1.

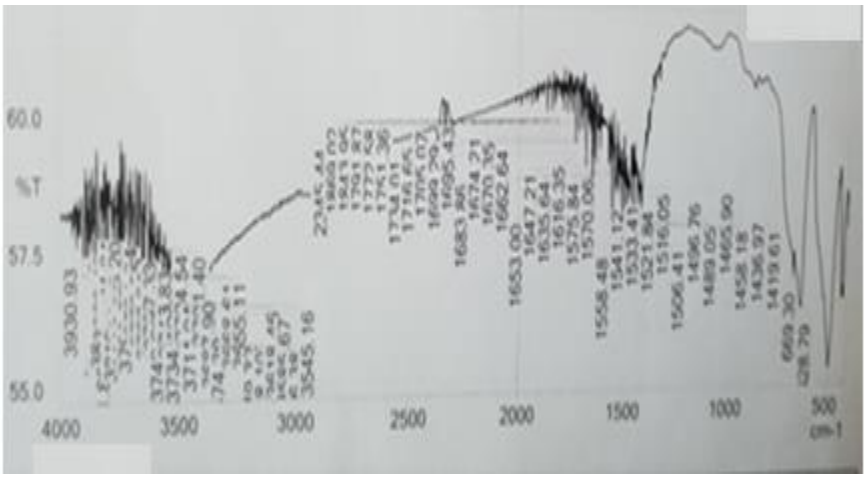


**Figure 4.3.** FT-IR spectrum of sample 2.

## 4.3 Uv-Vis absorption results of the synthesized $MgCr_2O_4$ samples

The optical band gap of the synthesized magnesium chromate samples was determined by ultraviolet visible (Uv-Vis) absorption technique. The optical absorption spectrum of the studied $MgCr_2O_4$ samples shows absorption peaks in the UV range as displayed in figure 4.4. There are three absorption peaks in the wavelength range. The peaks at about 275 and 375 nm of the spectrum can be indexed as two typical bands of octahedral $Cr^{+3}$ ions. They have been assigned to d–d transitions. The strong peak in the UV region could be attributed to band gap absorption of the $MgCr_2O_4$ nanocrystals (Cheng, P. and Lian, G. 2008). The prominent peak in the UV region could be attributed to band gap absorption of the $MgCr_2O_4$ samples (Atkins, P. W. et al. 2013). The optical band gap ($E_g$) of synthesized samples can be calculated using the optical absorption spectrum based on equation 2.7.

The optical band gap for the absorption peak can be deducted by extrapolating the linear portion of the $(A\upsilon)^2$ vs $\upsilon$ curve to zero as seen in figure 4.5 linear relation was observed from the function curve of $(A\upsilon)^2$ vs $\upsilon$. This indicates that the as prepared $MgCr_2O_4$ samples possess a direct optical band gap. The calculated band gaps were 3.007 eV and 3.057 eV for the sample 1 and sample 2, respectively. The energy band gap of the sample 2 was greater compared to the sample 1. This associate to values of crystallite sizes obtained from XRD results.

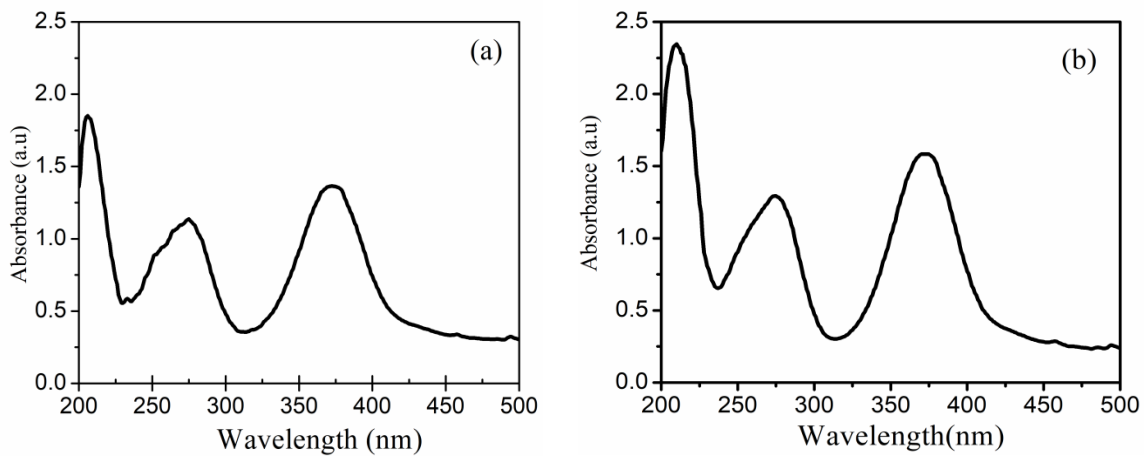


**Figure 4.4.** Uv-Vis absorption spectrum of (a) sample 1 and (b) sample 2.

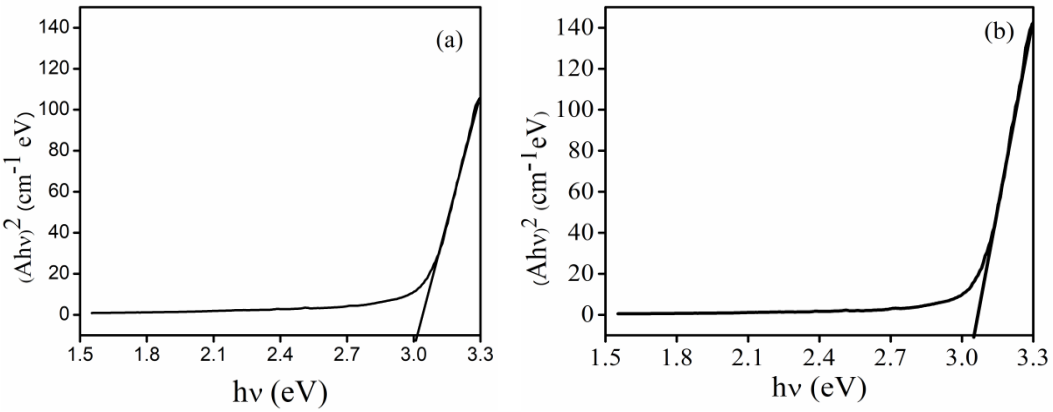


**Figure 4.5.**The $(Ah\upsilon)^2$ vs $h\upsilon$ curve (a) sample 1 and (b) sample 2.

## 4.4 Conclusions

Two samples of spinel magnesium chromate ($MgCr_2O_4$) were synthesized by combustion method. Sample 1 was prepared without ammonium hydroxide and produced within 2:10 h whilst sample 2 was prepared by adding ammonium hydroxide and produced within 45 minutes. The influence of the synthesis methods on the structural and optical properties of samples was investigated. The crystalline phase of the magnesium chromate samples was identified using the X-rays diffraction spectroscopy. The XRD results show that sample 1 was more crystalline and possesses large value of crystallite sizes compared to sample 2. Furthermore, the average crystallite sizes was determined using Scherer's formula and found to be 13 and 8 nm for sample 1 and sample 2, respectively. The existence of metal oxide bonds at both samples was confirmed using Fourier transform infrared (FT-IR) spectroscopy technique. The optical absorption of the ultraviolet-visible (Uv-Vis) spectrum of the $MgCr_2O_4$ samples shows the absorption peaks in the UV wavelength range. The calculated band gap values were 3.007 eV and 3.057 eV for the sample 1 and sample 2, respectively.

Adding ammonium hydroxide reduced time of synthesis process and produced sample with small value of crystallite sizes. However, calcination can be achieved to improve the crystalline phase of the synthesized sample.

## 4.5 Recommendations

In this study, some recommendations can be suggested which may lead to best results for a similar study

- Additional information about structure such as atoms position and

molecule bonding can obtained by fitting XRD patterns using full proof software program.

-The particle sizes and morphology of the synthesized samples can be studied using high resolution transmission electronic microscopy (HRTEM) and high resolution scanning electron microscope (HRSEM).

## 4.6 Future work

For any advance study, the following notes should be considered, so it can contribute a new finding of interest as well as to understand the new properties of magnesium chromates nanocrystals.

- Effect of annealing treatment on structure and optical properties of the synthesized sample can be investigated.
- The anticorrosion property of the synthesized magnesium chromate can be examined.

## Reference


Adair, J. H., Kerchner, J. A., Bell, N. S. and Carasso, M. L. (1998). Application of chemical principles in the solution synthesis and processing of ceramic and metal particles, Synthesis and Characterization of Advanced Materials**,** vol. 681, pp. 82-94.

Ahmed, A. M. (2011). Ab initio large unit cell calculation of the electronic structure of diamond nanocrystals. Bibcode: 2011SSSci.13.843A. Solid state sciences, vol. 5, no.13, pp.843.

Armendariz, V. Herrera, I. and Peralta-Videa, J. R. (2004). Size controlled gold nanoparticle formation by Avena sativa. Biomass: use of plants in nanobiotechnology. Journal of Nanoparticle Research, vol. 6, no. 4, pp. 377–382.

Atkins, P. W. and Paula, J. D. (2013). Physikalische Chemie, 5th ed, Wiley - VCH, Weinheim.

Baker, S. Rakshith, D. and Kavitha, K. S. (2014). nanofactories towards facile route in synthesis of nanoparticles, Plants: emerging. Journal BioImpacts, vol. 3, no. 3, pp. 111–117.

Barhoum, J. A., Chan, Y. S., Dufresne, A. and Danquah, K. (2018). Nanomaterial classification regulations Beilstein: Journal nanotechnol, Published: 3 April. 9, pp. 1050–1074. Doi:10.3762/bjnano.9.98.

Bates, J. L. and Gamier, J. E. (1981). Electrical conductivity of $MgAl_2O_4$ and $Y_3A1_5O_{12}$, Journal of the American Ceramic Society, vol. 64, doi.org/10.1111/j.1151-2916.1981.tb10237.x.

Bawendi, M. G., Steigenvald, M. L., Brus, L. E., Weller, H. Schmidt, H. M., Koch, U. Foitik, A. and Baral, S. (1990). Annu: Reu. Journal Physical Chemical, vol. 485, no. 41, pp. 477.

Boholm, M. n. and Boholm, A. M. (2012). The many faces of nano in newspaper reporting, Journal Nanoparticle Res, vol.14, pp.722-740.

Brindley, G. W. and Brown, G. (1980). Crystal Structures of Clay Minerals and their Identification. Mineralogical Society: London. Vol. 44, pp. 363.

Burdett, J. K., Price, G. L. and Price, S. L. (1982). Role of the crystal-field theory in determining the structures of spinel. Journal Am. Chem. Soc. vol. 10, pp. 92-95. Doi: 10.1021/ja00365a019,

Burt, J. L. (2005). Beyond Archimedean solids: Star polyhedral gold nanocrystals. J. Crystal Growth, vol. 285, no. 4 pp. 681-691.

Chen, H. M. and Liu, R. S. (2011). Architecture of metallic nanostructures: synthesis strategy and specific applications. The Journal of Physical Chemistry, vol. 115, pp. 3513-3527.

Cheng, P. and Lian, G. (2008). Optical and photocatalytic properties of spinel $ZnCr_2O_4$ nanoparticles synthesized by hydrothermal route. Journal American ceramic society, vol. 91, no. 7, pp. 2388-2390.

Cui, H. Abu-Siada, A. Li. S. and Islam, S. (2017). Correlation between dissolved gases and oil spectral response: Proceedings of the 1st International Conference on Electrical Materials and Power Equipment-Xian Jiaotong University, China, pp. 14–17.

Fahlman, B. D. (2007). Material Chemistry: Springer, Berlin, pp. 282–283. Doi:10.1007/978-1-4020-6120-2.

Ghead, K. S. and Saja, M. J. (2016). The Effect of pH on Partial Size of Ferrimagnetic Powders Prepared by Auto Combustion Method. Nanotechnology and Advanced Materials Research Center: University of Engineering Technology, Baghdad Journal, vol. 34, no. 2, pp.269-277.

Gorter, E. W. (1954). Saturation magnetization and crystal chemistry of ferrimagnetic oxides, Rijksuniversiteitte Leiden.

Gratzel, M. (1988). Heterogeneous Photochemical Electron Transfer, CRC Press 1st Edition.

Grunes, L. A. (1983). Study of the K edges of 3 d transition metals in pure and oxide form by x-ray-absorption spectroscopy, Physical Review B 27, 21.

Grimes, N. W. (1983). New symmetry and structure for spinel. Proceedings of: the Royal society of London Series. A Mathematical and Physical Sciences, vol. 386, no.1791, pp. 333-345.

Hamed, F. Tholkappiyan, R. and Vishista, K. (2016). The effect of induced strains on the optical band gaps in lanthanum doped zinc ferrite nanocrystalline powders, Mod: Physic, B 30, no.1650230.

Hodak, J. Martini, I. and Hartland, G. V. (1998). Chemical Phys. Lett. 284, pp. 135.

Houshiar, M. Askari, Z. Zebhi, F. and Alidoust, A. (2013). In the Proceeding Conference of Physics Society of Iran, pp. 1134–1137.

Jafarnejada, E. Khanahmadzadeha, S. Ghanbarya, F. and Enhessarib, M. (2016). Synthesis, characterization and optical band gap of Pirochromite ($MgCr_2O_4$) Nanoparticles by Stearic Acid Sol-Gel Method, Current Chemistry Letters 5, 11 July, 173–180.

Johnston, D. Prakash, H. Zachariasen, W. and Viswanathan, R. (1973). High temperature superconductivity in the Li-Ti-O ternary system. Materials Research Bulletin, vol. 8, pp. 777-784.

Kakani, S. L. and Kakani, A. (2004). New Age International (P) Limited. Publishers, Ansari Road, Daryaganj, New Delhi, vol. 483, 110002.

Loría-Bastarrache, W. Herrera-Kao, J. and Cauich-Rodríguez, J. V.(2011). Journal of thermal analysis and calorimetry vol. 104, no. 2, pp. 737-742.

Manh, D. H., Thuan, N. C., Phong, P. T., Hong, L. V., and Phuc, N. X. (2009). Magnetic properties of La0.7Ca0.3MnO3 nanoparticles prepared byreactive milling. Journal of Alloys and Compounds, vol. 479, pp. 828-831.

Manjon, F. J., Tiginyanu, I. and Ursaki, V. (2014). Pressure-Induced Phase Transitions in $AB_2X_4$. Chalcogenide Compounds: Springer series in materials science. 189.

Mariappan, R. Ponnuswamy, V. Ragavendar, M. Krishnamoorthi, D. and Sankar, C. (2012). The effect of annealing temperature on structural and optical properties of undoped and Cu doped CdS thin films Optik-Int. Journal Light Electron Opt, vol.123, PP.1098–102.

Nakamoto, K. John, W. and Sons, I. (1963). Infrared Spectra of Inorganic and Coordination Compounds. Journal of pharmaceutical sciences, vol. 52, no.8 Wiley, New York, pp.77.

Roco, M. C., Williams, R. S. and Alivisatos, P. (1999). Nanotechnology Research Directions: IWGN Research Report. Committee on Technology, Interagency Working Group on Nanoscience, Engineering and Technology (IWGN), National Science and Technology Council.

Rotello, V. M. (2004). Nanoparticles: Building Blocks for Nanotechnology, Publisher Springer US.

Ramachandran, T. and Hamed, F. (2016). Synthesis of nanostructured pirochromite magnesium chromate with egg shell membrane template, Published: 11 August in Springer link. Com, v. 6, pp. 1233–1246. Doi: 10.1007/s13204-016-0538-7

Salahudeen, A. G., Saion, E. Shaari, A. Mazliana, A. K., Naif, M. A. and Kharazmi, A. (2014). Structural, Optical and magnetic characterization of spinel Zinc chromite of nanocrystals synthesized by treatment method. Journal of nanomaterials , no. 3. Doi: 10.1155/2014/416765.

Sanjeeviraja, G. and Kalai, S. (2013). Investigations on the temperature dependent electrical and magnetic, properties of $NiTiO_3$ by molten saltsynthesis. Mater. Res. Bull, vol. 4, no.8, pp. 1110–1116.

Shapira, P. and Jan, Y. (2011). Introduction to the symposium issue: nanotechnology innovation and policycurrent strategies and future trajectories. The Journal of Technology Transfer, vol. 36, no.6, pp. 581-586.

Smith, J. and Wijn, H. (1959). Ferrites: Philips Technical Library, Eindhoven, 150.

Smith, R. A. (1978). Semiconductors second edit. New York: Cambridge University Press.

Stanojević, Z. M., Romčević, N. and Stojanović, B. (2007). Spectroscopic study of spinel $ZnCr_2O_4$ obtained from mechanically activated $ZnO$-$Cr_2O_3$ mixtures, Journal of the European Ceramic Society, vol. 27, pp. 903-907.

Sumaira, N. (2016). Synthesis and characterization of nanocrystalline transition metal oxides, chromites and ferrites. National Centre for Nanotechnology Department of Metallurgy and Materials Engineering Pakistan Institute of Engineering and Applied Sciences Nilore, Islamabad, Pakistan, June.

Suzuki, N. Tanaka, H. and Kawai, T. (2008). Epitaxial Transition Metal Oxide Nanostructures Fabricated by a Combination of AFM Lithography and Molybdenum Lift-Off Advanced Materials, vol. 20, pp. 909-913.

Tauc, J. (1974). In: Amorphous and Liquid Semiconductors, ed. Plenum, London, pp. 175.

Ueda, N. Omata, T. N., Hikuma, K. Ueda, H. Mizoguchi, T. and Hashimoto, H. (1992). New oxide phase with wide band gap and high electro conductivity $MgIn_2O_4$, Journal Applied physics letters, vol. 61, pp. 1954-1955.

Weckhuysen, B. M., Wachs, I. E. and Schoonheydt, R. A. (1996). Surface Chemistry and Spectroscopy of Chromium in Inorganic Oxides. Chem Rev, vol. 96, no. 3327, pp. 50.

White, A. D. (2006). High pressure study of spinel chromite (Doctoral dissertation).

Wolcott, A. Gerion, D. Visconte, M. Sun, J. Schwartzberg, A. Chen, S. W. and Zhang, J. Z. (2006). Journal Physical Chem. Vol. 110, pp. 5779.

Wurschum, R. and Schaefer, H. E.(1996). Nanomaterials Synthesis, Properties, and Applications, Eds Edelstein AS and Cammarata RC. Bristol: Institute Physics, vol. 277.

Xinyuan, Z. Wei, C. M., Yang, L. and Chou, M. Y. (2004). Quantum Confinement and Electronic Properties of silicon Nanowires .Published 11 June, Phys. Rev, Lett.92, 236805, vol. 9, no.12, pp. 596.